Atmos. Chem. Phys. Discuss., https://doi.org/10.5194/acp-2018-755
Manuscript under review for journal Atmos. Chem. Phys.
Discussion started: 6 August 2018

Atmospheric Chemistry and Physics Discussions

New insights into OH airglow modelling to derive night-time atomic oxygen and atomic hydrogen in the mesopause region

Tilo Fytterer[1], Christian von Savigny[2], Martin Mlynczak[3], Miriam Sinnhuber[1]

[1]Institute for Meteorology and Climate Research, Karlsruhe Institute of Technology, Eggenstein-Leopoldshafen, 76344, Germany

[2]Institute of Physics, University of Greifswald, Greifswald, 17489, Germany

[3]NASA, Langley Research Center, Hampton, Virginia, 23681-2199, USA

Correspondence to: Miriam Sinnhuber (miriam.sinnhuber@kit.edu)

Abstract. An OH airglow model was developed to derive night-time atomic oxygen ($O(^3P)$) and atomic hydrogen (H) from satellite OH airglow observations in the mesopause region (~75-100 km). The OH airglow model is based on the zero dimensional box model CAABA/MECCA-3.72f and was empirically adjusted to fit four different OH airglow emissions observed by the satellite/instrument configuration TIMED/SABER at 2.0 µm and at 1.6 µm as well as measurements by ENVISAT/SCIAMACHY of the transitions OH(6-2) and OH(3-1). Comparisons between the "Best fit model" obtained here and the satellite measurements suggest that deactivation of vibrationally excited OH(ν) via $OH(\nu\geq7)+O_2$ might favour relaxation to $OH(\nu'\leq5)+O_2$ by multi-quantum quenching. It is further indicated that the deactivation pathway to $OH(\nu'=\nu-5)+O_2$ dominates. The results also provide general support of the recently proposed mechanism $OH(\nu)+O(^3P)\rightarrow OH(0\leq\nu'\leq\nu-5)+O(^1D)$ but suggest slower rates of $OH(\nu=7,6,5)+O(^3P)$. Additionally, deactivation to $OH(\nu'=\nu-5)+O(^1D)$ might be preferred. The profiles of $O(^3P)$ and H derived here are plausible between 80 km and 95 km. The values of $O(^3P)$ obtained in this study agree with the corresponding TIMED/SABER values between 80 km and 85 km, but are larger from 85 to 95 km due to different relaxation assumptions of $OH(\nu)+O(^3P)$. The H profile found here is generally larger than TIMED/SABER H by about 30-35 % from 80 to 95 km, which might be attributed to too high O_3 night-time values.

1 Introduction

Atmos. Chem. Phys. Discuss., https://doi.org/10.5194/acp-2018-755
Manuscript under review for journal Atmos. Chem. Phys.
Discussion started: 6 August 2018

Atomic oxygen in its ground state ($O(^3P)$) and atomic hydrogen (H) strongly influence the energy budget in the mesopause region (~75-100 km) during day and night, and consequently affect atmospheric air temperature, wind, and wave propagation. Therefore, an improved knowledge of the abundance of $O(^3P)$ and H is of great importance when studying the mesopause region. At these altitudes, $O(^3P)$ has a direct impact on the heating rates by participating in several exothermic chemical reactions (Mlynczak and Solomon, 1993, their Table 4). But $O(^3P)$ also contributes to radiative cooling by exciting CO_2 via collisions, leading to increased infrared emissions of CO_2 and partly opposing the $O(^3P)$ chemical heating effect. Night-time H plays a crucial role in the mesopause region due to the destruction of ozone (O_3) which is accompanied by the release of a considerable amount of heat (Mlynczak and Solomon, 1993). This chemical reaction additionally leads to the production of excited hydroxyl radicals (OH(ν)) up to the vibrational level ν=9, causing the formation of OH emission layers in the atmosphere (Meinel bands; Meinel, 1950).

Direct measurements of $O(^3P)$ and H are relatively rare because as atomic species they do not have observable vibration-rotation spectra. Consequently, measuring these species in the mesopause region by remote sensing requires complex methods while in situ observations are rather expensive (e.g. Mlynczak et al., 2004; Sharp and Kita, 1987). Thus, there exists no global data set based on direct observations. As a consequence, an indirect method was introduced by Good (1976) to derive $O(^3P)$ and H during night, using OH airglow emissions. This approach was also adapted by Mlynczak et al. (2013; 2014; 2018) which derived a global data set of night-time $O(^3P)$ and H in the mesopause region from satellite observations of OH(ν). The method is based on the assumption of chemical steady state of O_3 and further depends on several radiative lifetimes, chemical reactions, and physical processes involving OH(ν). However, the corresponding total rate coefficients and branching ratios are still not sufficiently known, and thus present a large source of uncertainty in the derivation of $O(^3P)$ and H.

There are two major issues currently discussed in the literature which considerably affect the overall abundance of derived $O(^3P)$ and H. The first problem addresses the underlying deactivation schemes of OH(ν) from the higher excited state ν to the lower excited state ν' ($\nu'<\nu$) by collisions with O_2. This can generally occur via sudden death ($OH(\nu)+O_2 \rightarrow OH(\nu'=0)+O_2$), single-quantum ($OH(\nu)+O_2 \rightarrow OH(\nu'=\nu-1)+O_2$), or multi-quantum ($OH(\nu)+O_2 \rightarrow OH(\nu'<\nu)+O_2$) quenching. However,

in case of the sudden death approach, it is still unknown where such a huge amount of excess energy is transferred. The second crucial point comprises the deactivation scheme and the total rate of $OH(v)+O(^3P)$, including the new pathway $OH(v)+O(^3P)\rightarrow OH(0\leq v'\leq v-5)+O(^1D)$ suggested by Sharma et al. (2015).

Over the last decades, several model studies attempted to fit OH airglow measurements, using different rates and schemes for the deactivation of OH(v) by O_2 and by $O(^3P)$. And at least to our knowledge, there is no general agreement about which model is correct. The deactivation of OH(v) by O_2 in many models (e.g. von Savigny et al., 2012; Mlynczak et al., 2013; Grygalashvyly et al., 2014; Panka et al., 2017) is based on the model proposed by Adler-Golden (1997). It assumes a combination of multi-quantum and single-quantum quenching and was derived from theoretical considerations and ground-based observations. Xu et al. (2012) investigated measurements of the Sounding of the Atmosphere using Broadband Emission Radiometry (SABER) instrument on board the NASA Thermosphere-Ionosphere-Mesosphere Energetics and Dynamics (TIMED) satellite of the OH airglow emissions at 2.0 µm and at 1.6 µm. Their results support the model of Adler-Golden (1997) but suggest slower total $OH(v)+O_2$ rates. They further exclude the sudden death mechanism as a possible deactivation scheme. There are also two theoretical studies (Shalashilin et al., 1995; Caridade et al., 2002) which investigated OH(v) deactivation via O_2, both supporting a combination of multi-quantum and single-quantum quenching similar to the model of Adler-Golden (1997).

However, Russell and Lowe (2003) and Russell et al. (2005) analyzed OH(8-3) and $O(^1S)$ airglow emissions measured by the Wind Imaging Interferometer (WINDII) instrument on board the Upper Atmospheric Research Satellite (UARS). Both airglow emissions were used to individually derive $O(^3P)$ and the best agreement between these two $O(^3P)$ profiles was obtained when a sudden death scheme for $OH(v)+O_2$ quenching was applied. Kaufmann et al. (2008) investigated several OH airglow spectra between 1 µm and 1.75 µm measured by the Scanning Imaging Absorption Spectrometer for Atmospheric Chartography (SCIAMACHY) instrument on board the Environmental Satellite (ENVISAT). They found best agreement between their model and the measured OH airglow spectra when a combination of sudden death and single-quantum quenching was used.

Vibrationally dependent rates of $OH(v)+O(^3P)$ were determined by Varandas (2004) and Caridade et al.

(2013), using quasi-classical trajectory calculations. Their results suggest that deactivation occurs via a chemical reaction as well as multi-quantum quenching. Kalogerakis et al. (2011) obtained a deactivation rate of OH(9) +O(^{3}P) from laboratory experiments which is several times larger than the rate from these calculations. But applying this fast quenching rate led to non-physical O(^{3}P) values and associated heating rates (Smith et al., 2010; Mlynczak et al., 2013). Thus, Sharma et al. (2015) proposed a new mechanism OH(v)+O(^{3}P)→OH(0≤v'≤v-5)+O(^{1}D) to account for results from both theory and experiment. Very recent laser experiments and model studies support this new pathway while the exact values of the branching ratios and total loss rates are still not known (Kalogerakis et al., 2016; Panka et al., 2017). However, recently published results by Mlynczak et al. (2018) oppose this mechanism. They also applied the new rate of Kalogerakis et al. (2011) for OH(9)+O(^{3}P). But in order to get the annual energy budget into near balance, it was necessary to assume that at least OH(9)+O(^{3}P) occurs via single-quantum relaxation. Additionally, the rate of OH(8)+O_2 had to be reduced and is considerably smaller than the value reported from Adler-Golden (1997).

In order to address the two major issues stated above, this paper is focused on the development of a zero dimensional box model for atmospheric OH airglow with the intention to derive night-time O(^{3}P) and H in the mesopause region. The model considers the formation of OH(v) via H+O_3 and deactivation of OH(v) due to spontaneous emission of photons, chemical reactions and physical collisions with atmospheric air compounds N_2, O_2, and O(^{3}P). We used the indirect method introduced by Good (1976) and derived night-time O(^{3}P) and H from TIMED/SABER OH emissions at ~2.0 µm, while also considering the OH airglow observations from TIMED/SABER at ~1.6 µm as well as the OH(6-2) and OH(3-1) transitions measured by ENVISAT/SCIAMACHY. Further sensitivity runs were carried out to estimate the uncertainty on the derived values of O(^{3}P) and H due to the different deactivation schemes, overall rate constants, and branching ratios.

2 Data and method

2.1 Satellite measurements

2.1.1 ENVISAT/SCIAMACHY

The SCIAMCHY instrument (Bovensmann et al., 1999) was an 8-channel spectrometer on board ENVISAT, providing atmospheric OH airglow emission measurements between ~220 nm and ~2380 nm. ENVISAT was launched into a polar and sun-synchronous orbit and crossed the equator at ~10 LT and ~22 LT. The ENVISAT mission started in March 2002 and SCIAMACHY was nearly continuously operating until the end of the mission in April 2012 caused by a spacecraft failure. The SCIAMACHY instrument performed measurements in different observations modes, including night-time (~22 LT) limb scans over the tangent altitude range ~75-150 km. These measurements are only available throughout the year at latitudes between the equator and 30° N.

In this paper, we used SCIAMACHY level 1b data v7.04 to retrieve OH airglow volume emission rates (VERs) of the OH(3-1) and OH(6-2) bands in the wavelength ranges of 1515-1546 nm and 837.5-848 nm, respectively. The retrieval approach applied here is very similar to the one described in von Savigny et al. (2012). The retrieval does not cover the complete spectra of the OH(3-1) and OH(6-2) bands, and consequently a "correction factor" of 2.48 for OH(3-1) VER and 2.54 for OH(6-2) VER was added to account for the entire band emissions at mesopause temperature. The data set further includes corrections for misalignments and other measurement errors (Gottwald et al., 2007). Investigations performed by Bramstedt et al. (2012) showed a drift of the SCIAMACHY tangent height of less than 20 m $year^{-1}$ which is negligible for our study.

The uncertainties of the OH(3-1) VER and OH(6-2) VER retrievals from SCIAMACHY limb observations correspond to the propagated uncertainties of the observed limb emission rate (LER) profiles. The latter are estimated from the LER values in the tangent height range between 110 km and 150 km, where the actual atmospheric emissions should be zero. The VER uncertainties are first determined for daily and zonally averaged data. The uncertainties used in this analysis correspond to the mean uncertainties averaged over all days with co-located SCIAMACHY and SABER observations.

2.1.2 TIMED/SABER

The SABER instrument (Russell et al., 1999) on board the TIMED satellite has been nearly continuously operating since January 2002, collecting over 98 % of all possible data. The instrument scans

the atmosphere from the surface up to altitudes of ~400 km while providing a vertical resolution of about 2 km throughout the entire height interval. Due to the geometry of the satellite orbit and the regular yaw manoeuvres every ~60-65 days, SABER only provides complete coverage of the latitude range between ~55° S and ~55° N. The SABER instrument measures the OH VERs at ~2.0 µm and at ~1.6 µm which approximately corresponds to the transitions of OH(9-7)+OH(8-6) and OH(5-3)+OH(4-2), respectively. The contribution of OH(7-5) to OH VER at 2.0 µm and of OH(3-1) to OH VER at 1.6 µm is only about a few percents (Xu et al., 2012; Mlynczak et al., 2013) and is neglected in this paper.

In this study, we used the SABER Level 2A data v2.0 of the "unfiltered" OH VERs at 2.0 µm and at 1.6 µm, the air temperature and pressure, and the volume mixing ratios (VMRs) of O_3 (derived at 9.6 µm). New night-time VMRs of $O(^3P)$ and H (Mlynczak et al., 2018) were used for comparison with the results derived from our model. The "unfilter" factor applied to OH VER adjusts the originally measured OH VER by the SABER instrument to the total VER emitted by OH in the corresponding vibrational bands, while considering the shape, width, and transmission of the SABER broadband filters (Mlynczak et al., 2005). Outliers were excluded by screening the data as suggested by Mlynczak et al. (2013). The SABER data used here were further restricted to observations between 21 LT and 23 LT to approximately match the SCIAMACHY measurement time at ~22 LT. In order to be consistent with the naming of the SCIAMACHY OH airglow observations, the SABER OH airglow at 2.0 µm and at 1.6 µm are referred to as OH(9-7)+OH(8-6) and as OH(5-3)+OH(4-2) throughout the paper.

2.2 Method

In order to minimize issues between SABER and SCIAMACHY due to different measurement characteristics, we focused on the latitude range from 0° to 10° N, which was covered by both instruments throughout the entire year. A broader latitude band is not recommended because SABER and SCIAMACHY do not uniformly cover the same latitudes, leading to disagreements between the real latitude of the observations and the nominal latitude of the interval. The accepted profiles of both instruments within the chosen latitude interval were averaged to zonal mean nightly mean values. All these zonal mean nightly means from January 2003 to December 2011 were used to calculate a climatology, including only days on which both SCIAMACHY and SABER data are available.

Atmos. Chem. Phys. Discuss., https://doi.org/10.5194/acp-2018-755
Manuscript under review for journal Atmos. Chem. Phys.
Discussion started: 6 August 2018

The approach to derive O(^{3}P) and H applied here was developed by Good (1976) and is described in detail in Mlynczak et al. (2013). Thus, we only give a brief summary here. The measured SABER OH(9-7)+OH(8-6) VER (photons cm^{-3} s^{-1}) is given by Eq. (1):

$$\mathrm{OH(9\text{-}7)+OH(8\text{-}6)\ VER} = k_1[\mathrm{H}][\mathrm{O_3}]\mathrm{G}(f_v, A_{vv'}, C_{vv'}), \qquad (1)$$

where k_1 is the rate constant of the chemical reaction H+O$_3$, representing direct production. The function G (Eq. (2)) comprises all relevant production and loss processes of OH(9-7) VER and OH(8-6) VER:

$$G = \frac{f_9}{A_9 + C_9} A_{97} + \frac{f_8}{A_8 + C_8} A_{86} + \frac{f_9}{A_9 + C_9} \frac{A_{98} + C_{98}}{A_8 + C_8} A_{86}, \qquad (2)$$

The subscripts v and v' (v'<v) are the vibrational states of OH before and after the corresponding process. The terms f_v are the nascent distributions and describe the production efficiency of OH(v) via the reaction H+O$_3$. Total radiative loss due to spontaneous emissions is considered by the Einstein coefficients A_v (s^{-1}) which are the inverse radiative life times of OH(v). The total loss rate C_v (s^{-1}) is the sum of loss due to collisions with the air compounds (N$_2$, O$_2$, O(^{3}P)), including chemical reactions and physical quenching. The terms $A_{vv'}$ and $C_{vv'}$ represent the specific state-to-state transitions.

In the second step, chemical equilibrium of O$_3$ during night is assumed as follows:

$$k_1[\mathrm{H}][\mathrm{O_3}] + k_2[\mathrm{O}(^3\mathrm{P})][\mathrm{O_3}] = k_3[\mathrm{O}(^3\mathrm{P})][\mathrm{O_2}][\mathrm{M}], \qquad (3)$$

meaning that O$_3$ loss due to H and O(^{3}P) (left side) is balanced by the three-body-reaction O(^{3}P)+O$_2$+M (right side). Here, k_2 and k_3 are the corresponding rate constants of O(^{3}P)+O$_3$ and O(^{3}P)+O$_2$+M, respectively, while M is the total number density of the air.

Finally, rewriting Eq. (1) enables the derivation of H while O(^{3}P) is calculated by substituting Eq. (3) in Eq. (1) and rewriting the resulting term as follows:

$$[\mathrm{H}] = \frac{\mathrm{OH(9-7)+OH(8-6)\ VER}}{\mathrm{G}\,k_1[\mathrm{O_3}]}, \qquad (4a)$$

$$[\mathrm{O}(^3\mathrm{P})] = \frac{\mathrm{OH(9-7)+OH(8-6)\ VER}}{\mathrm{G}\,(k_3[\mathrm{O_2}][\mathrm{M}] - k_2[\mathrm{O_3}])}. \qquad (4b)$$

Air temperature and air pressure from SABER were used to calculate M as well as the number densities of O$_2$ (VMR of 0.21), N$_2$ (VMR of 0.78), and SABER O$_3$ via the ideal gas law. The chemical reaction

rates and physical quenching processes involved are described in Sect. 2.3. The values of $O(^3P)$ and H were individually derived for each altitude. Finally, the obtained vertical profiles of $O(^3P)$ and H were used to initialize the OH airglow model (see Sect. 2.3).

It is apparent from Eq. (4a-b) that any changes applied to the input parameters (G, O_2, O_3, M, k_1, k_2, k_3) are balanced by the derived values of $O(^3P)$ and H. In contrast, OH(9-7)+OH(8-6) VER is not affected by the input parameters and therefore identical in every model run. However, the goal of this paper is to develop a model which does not only fit OH(9-7)+OH(8-6) VER observations but also reproduces the three other airglow measurements OH(6-2) VER, OH(5-3)+OH(4-2) VER, and OH(3-1) VER. We have to further point out, that the relation between $O(^3P)$ and OH(9-7)+OH(8-6) VER is not linear since the function G also depends on $O(^3P)$, as represented by the terms C_ν and $C_{\nu\nu'}$. In fact, Eq. (4b) is a quadratic expression with respect to $O(^3P)$ but treated here as a linear one, making no substantial differences for small $O(^3P)$. Nevertheless, this issue is addressed in detail in Sect. 3.4.

2.3 The OH airglow Base model

The model used in this study is based on the atmospheric chemistry box model Module Efficiently Calculating the Chemistry of the Atmosphere/Chemistry As A Box model Application (MECCA/CAABA-3.72f; Sander et al., 2011). The box model calculates the temporal evolution of chemical species inside a single air parcel of a certain pressure and temperature, making the model very suited for sensitivity studies. The CAABA/MECCA standard model was extended by several chemical reactions and physical quenching processes involving OH(ν) which are described in this section. The model was run until it reaches steady-state, defined by the agreement between the measured and modelled OH(9-7)+OH(8-6) VER.

The OH airglow model described in this section is referred to as “Base model” because it is the starting point of our model studies. But we have to point out that there is no such a thing as a commonly accepted OH airglow base model in the literature. The Base model takes into account all major formation and loss processes of OH(ν) (Table 1) which are commonly used in other models in the literature and are assumed not to be seriously in error. The model comprises the production of OH(ν) via the chemical reaction $H+O_3$ as well as the deactivation due to spontaneous emission and the removal

physical quenching and chemical reactions with N_2, O_2, and $O(^3P)$.

The chemical reactions $H+O_3$, $O(^3P)+O_3$, and $O(^3P)+O_2+M$ were already included in the CAABA/MECCA standard model and their corresponding rates were taken from the latest Jet Propulsion Laboratory (JPL) report 18 (Burkholder et al., 2015). The reaction $H+O_3$ populates OH up to the vibrational level $v\leq9$ and the nascent distribution of OH(v) was taken from Adler-Golden (1997). The spontaneous emissions are given by the Einstein coefficients at 200 K (Xu et al., 2012). Deactivation of OH(v) by N_2 is assumed to occur via single-quantum quenching. The rates at room temperature for OH($v\leq8$) and for OH($v=9$) were taken from Adler-Golden (1997) and Kalogerakis et al. (2011), respectively.

Quenching of OH(v) by O_2 is based on the values reported by Adler-Golden (1997, their Table 3) which comprise a combination of multi-quantum and single-quantum quenching. However, Adler-Golden (1997) applied a factor of ~1.5 to account for mesopause temperature based on comparisons between laboratory measurements at room temperature of $OH(8)+O_2$ and the corresponding rate inferred from OH(8-3) rocket observations in the mesopause region. But later experiments reported by Lacousiere et al. (2003) and calculations by Caridade et al. (2002) suggest smaller values. The latter study further indicates that the temperature dependence decreases for lower vibrational levels and becomes negligible for OH($v\leq4$). Consequently, the rates presented in Adler-Golden (1997) were scaled to room temperature measurements ($v=1$-6 Dodd et al., 1991; $v=7$ Knutsen et al., 1996; $v=8$ Dyer et al., 1997; $v=9$ Kalogerakis et al., 2011), and afterwards a factor of 1.1 for OH($v\geq6$) and 1.05 for OH(5) was added.

The removal of OH(v) via collisions with $O(^3P)$ is included by using a combination of multi-quantum quenching (Caridade et al., 2013, their Table 1) and chemical reactions (Varandas, 2004). The rates were obtained from quasi-classical trajectory calculations at 210 K, approximately matching mesopause temperature.

3 Results and discussions

Figure 1 displays vertical profiles of a) OH(6-2) VER, b) OH(5-3)+OH(4-2) VER, and c) OH(3-1)

VER, comparing the observations (black squares) with the corresponding Base model output (red line). The model results of OH(6-2) VER and OH(3-1) VER are a 4 km running average to take the averaging kernels of SCIAMACHY measurements into account. The Base model approximately matches the general shape of the measured profiles but overestimates the three OH airglow measurements at the altitude of maximum VER. A closer look at the relative differences shows that the ratio model/observation at the altitude of maximum VER is about 2.0, 1.2, and 1.3 for OH(6-2), OH(5-3)+OH(4-2), and OH(3-1), respectively. Furthermore, these ratios increase with decreasing altitude, indicating that the overestimation of the Base model might be associated with O_2 quenching.

The differences between Base model and observations are quite substantial in case of OH(6-2) VER. This implies a general problem of the rates or schemes included in the Base model, requiring a detailed error analysis. The focus was set on potential error sources of OH(6-2) VER because the relative differences between model and measurements are largest compared to the other two OH transitions, and secondly because changes of OH(6) will affect the lower vibrational levels, but not vice versa.

3.1 Potential error sources of OH(6-2) VER in the Base model

Based on the results presented in Fig. 1, the potential error source has to have an effect on the entire height interval and must have a stronger impact on OH(6-2) compared to the other two OH transitions. We further focus on quantities with large uncertainties. For the latter reason, temperature is excluded as possible source because to account for a reduction of OH(6-2) VER by a factor of 2, temperature must be increased by more than 20 K (not shown here). Such a large error is very unlikely considering that a zonal mean climatology (2003-2011) is used here.

Since the overestimation of the Base model is especially large for OH(6-2) VER, an impact of the Einstein coefficient of the corresponding transition must be considered. Regarding this aspect, we have to point out that studies based on HITRAN 2004 data set should be viewed more critically, because of erroneous OH transition probabilities. The Einstein coefficients used in this study were recently recalculated (Xu et al., 2012, their Table A1) and correspond to a temperature of 200 K, which is very close to mesopause temperature. Furthermore, these Einstein coefficients are consistent with the values of the HITRAN 2008 data set (Rothman et al., 2009), Turnbull and Lowe (1989) after the correction

suggested by Adler-Golden (1997) is applied, and Nelson et al. (1990) which are applied to derive new night-time O(^{3}P) and H from SABER (Mlynczak et al., 2018). Therefore, an error of a factor of 2 for the transition of OH(6-2) is rather unlikely. Consequently, we exclude the Einstein coefficients as a potential fundamental error source.

The nascent distribution of the excited OH states of the chemical reaction H+O_3 was observed in several studies and all of them agree that OH(ν) is primarily formed in the vibrational levels ν=8 and ν=9 (e.g. Charters et al., 1971; Streit and Johnston, 1976; Ohoyama et al., 1985; Klenerman and Smith, 1987). The values used in the Base model were taken from Adler-Golden (1997) which are based on measurements reported by Charters et al. (1971) and agree with values obtained by Klenerman and Smith (1987) and Streit and Johnston (1976). The values found by Ohoyama et al. (1985) show some differences, but according to Klenerman and Smith (1987), their results are fundamentally flawed. This also affects the nascent distribution used by Mlynczak and Solomon (1993) which is an average of Charters et al. (1971), Ohoyama et al. (1985), and Klenerman and Smith (1987).

Therefore, we think that our nascent distribution used here is likely not a serious error source. However, minor errors might be introduced by extrapolating the nascent distribution to lower vibrational levels as it was done for the values used in our study (Adler-Golden, 1997). It is also possible that part of the nascent value of OH(6) is not due to direct production via H+O_3 but results from contributions of OH(ν≥7). In order to test the potential impact of the OH(6) nascent value on OH(6-2) VER, we assumed an extreme scenario by reducing the OH(6) nascent value from 0.03 to zero. But the corresponding results of OH(6-2) VER of the Base model run (not shown here) are only about 15 % lower compared to the values presented in Fig. 1. Further sensitivity runs also showed that an increase of the ratio f_9/f_8 is associated with a decrease of modelled OH(6-2) VER but even the extreme case of f_9=1 and f_8=0 could not account for a factor of 2. Note that changes of the overall rate constant of H+O_3 affect all considered OH transitions in a similar way, Thus, we conclude that direct production of OH(ν) is unlikely to be the reason for the overestimation of OH(6-2) VER by the Base model.

The physical removal of OH(ν) by N_2 is included as single-quantum relaxation which is supported by theoretical studies (Shalashilin et al., 1992; Adler-Golden, 1997). Assuming a sudden death scheme with the same overall deactivation rates resulted in a decrease of simulated OH(6-2) VER by less than 10 %

at the altitude of maximum VER. The total deactivation rate for OH(9) used here is about 1.5 times higher than the one suggested by Adler-Golden (1997) but the difference between the corresponding model OH(6-2) VERs is negligible (<1 %). There are two studies reporting temperature dependence of N_2 quenching (Shalashilin et al., 1992; Burtt and Sharma, 2008), both agreeing with measurements at room temperature. However, the calculations of the former study imply slower quenching rates at mesopause temperature compared to their respective values at room temperature whereas the latter publication indicates the opposite behaviour, reporting a ratio between the rate at 200 K and 300 K of approximately 1.7 for OH(v=8) and 1.3 for OH(v=9). These factors are generally supported by López-Puertas et al. (2004) which applied an empirically determined factor of 1.4 to the rates of Adler-Golden (1997) to account for mesopause temperature. Since the temperature dependence is still uncertain, we tested both possibilities. We increased and decreased the overall OH(v)+N_2 quenching rates by a factor of 1.5 which led to higher or lower OH(6-2) VERs by about 5 %. Therefore, N_2 is too inefficient as a OH(v) quenching partner to cause differences of OH(6-2) VER of a factor of 2.

The overall rate and exact pathways of OH(v)+O(^{3}P) are also still not known well enough but O(^{3}P) has nearly no influence on OH(v) at altitudes below 85 km. It therefore cannot be the only reason for the differences presented in Fig. 1. Consequently, deactivation by O_2 is the only remaining candidate which has a crucial influence on OH(v) throughout the entire height interval. Therefore, we will first focus on OH(v)+O_2 (Sect. 3.2) before investigating a potential influence of O(^{3}P) on OH(v) in Sect. 3.3.

3.2 Deactivation of OH(v) by O_2

The overestimation of OH(6-2) VER by the Base model can be generally corrected either by slower rates of OH(9,8,7)+O_2 or by a faster rate of OH(6)+O_2. The overall deactivation of OH(9) was measured by Chalamala and Copeland (1993) and they recommended a value of 2.1×10^{-11} cm^3 s^{-1}. This result was later confirmed by Kalogerakis et al. (2011), reporting a rate of 2.2×10^{-11} cm^3 s^{-1}. The rates for OH(8,7,6)+O_2 are each based on a single study only (v=8 Dyer et al., 1997; v=7 Knutsen et al., 1996; v=6 Dodd et al., 1991). But at least to our knowledge, there are no signs that the rates of OH(9,8,7,6)+O_2 are fundamentally flawed. In order to test the impact of the individual rates on OH(6-2) VER, we carried out sensitivity runs by varying the overall rates within their recommended 2σ errors.

Thus, we reduced the values of OH(9,8,7)+O_2 to 16×10^{-12} cm^3 s^{-1}, 7×10^{-12} cm^3 s^{-1}, and 5×10^{-12} cm^3 s^{-1}, respectively, while the rate of OH(6)+O_2 was increased to 4.5×10^{-12} cm^3 s^{-1}. But even under this favoured condition, the Base model output of OH(6-2) VER decreased only by a factor of 1.5, still not close to the required difference of a factor of 2. Additionally, the assumed scenario is rather unlikely since the overall rates were obtained by independent studies.

The possibility of a systematic offset of OH($v\leq6$)+O_2 rates, which are based on the single study (Dodd et al., 1991), is also excluded because of the very good agreement of this OH(2)+O_2 rate with the value obtained by Rensberger et al. (1989). Furthermore, when we increased the OH($v\leq6$)+O_2 rates by a factor of 3, the Base model approximately fits OH(6-2) VER and OH(3-1) VER but underestimates OH(5-3)+OH(4-2) VER by more than 30 %. Temperature dependence also affects the O_2 deactivation rates used here. But the factor to account for mesopause region temperature is suggested to be lower than 1.3 (Lacousiere et al., 2003; Cadidade et al., 2002) which has a weaker impact on OH(6-2) VER than the scenarios considered above.

Consequently, when applying the standard deactivations rates and schemes found in the literature, neither errors of the overall rates nor uncertainties of the temperature dependence can give a reasonable explanation of the overestimation of OH(6-2) VER Base model output shown in Fig. 1a. Since the overall rates were actually measured while the deactivation schemes are solely based on theoretical considerations, it is more convincing that the potential error source probably lies within OH(v)+O_2 deactivation scheme rather than in the deactivation rates.

In order to considerably reduce OH(6-2) VER, we assumed an extreme scenario and substituted the multi-quantum relaxation (OH(v)+O_2→OH($v'<v$)+O_2) in the Base model by a sudden death (OH(v)+O_2→OH+O_2) approach. This new model is referred to as "O_2 SD model" and the corresponding results are displayed in Fig. 2 as red lines, showing that the simulated OH(6-2) VER matches the observations within the error bars below 85 km. The model still overestimates the measurements in the altitude region above which might be related to O(^{3}P) quenching (see Sect. 3.3). The O_2 SD model output for the other two OH transitions (Fig. 2b-c) is clearly too low, implying that OH(v)+O_2 quenching cannot occur via sudden death alone. We also conclude that the contribution of higher excited states OH($v\geq7$) to OH(6) must be negligible or even zero and these higher states are

suggested to primarily populate lower vibrational levels OH(v≤5). Therefore, OH(v)+O_2 has to occur via multi-quantum quenching because in case of single-quantum deactivation the contribution of OH(v≥7) to OH(6) is considerably larger than zero.

According to Finlayson-Pitts and Kleindienst (1981), OH(v) might be relaxing to v'=v-5 while the excess energy is transferred to form $O_2(b^1\Sigma)$. This vibration-to-electronic energy transfer was also mentioned by Anlauf et al. (1968) and is supported by the close energy match of the transition from OH(9) to OH(4) and from $O_2(X^3\Sigma)$ to $O_2(b^1\Sigma)$ of about 36.6 kcal mol^{-1} and 37.5 kcal mol^{-1}, respectively. Although there is no experimental support of this deactivation pathway, this approach gives a reasonable explanation for the observed pattern in our study and OH(v) as a potential source of excited O_2 was discussed in Howell et al. (1990) and Murtagh et al. (1990). However, evaluating whether the product is really $O_2(b^1\Sigma)$ or another excited O_2 state is beyond the scope of this study. Thus, we concluded that deactivation of OH(v) by O_2 has to satisfy the following condition:

OH(v≥6)+O_2 → OH(0≤v'≤v-5)+O_2 (R8)

while we further assume that the pathway

OH(v≥6)+O_2 → OH(v'=v-5)+O_2 (R9)

is the preferred deactivation channel.

In order to test whether R9 could be the only pathway of R8 we assumed multi-quantum relaxation via:

OH(v)+O_2 → OH(v-5)+O_2 (R10a)

or OH(v)+O_2 → OH(v-4)+O_2 (R10b).

If R10a is integrated in the model (Fig. 2b-c, O_2 v-5 model), the corresponding model output at altitudes <90 km is only about 10 % below the observations of OH(5-3)+OH(4-2) VER and approximately matches OH(3-1) VER measurements within the error bars. The underestimation of the OH(5-3)+OH(4-2) VER measurements by the model could be attributed to minor errors of the OH(v)+O_2 overall rates in combination with a slightly different OH(v) branching of H+O_3. Therefore, we cannot completely rule out R10a as a possible solution, even if there are still some differences between the modelled and the observed OH VER. Including R10b in the model (Fig. 2b-c, O_2 v-4 model) results in an overestimation of the observations of OH(5-3)+OH(4-2) VER and OH(3-1) VER by about 20 % to 30 %, and

consequently this assumption is not further considered as a potential solution.

The results shown in Fig. 2 suggest that the OH airglow model is not able to reproduce the three OH airglow observations when sudden death or simplified multi-quantum schemes for OH(ν)+O_2 are applied. But the O_2 ν-5 model output is quite close to the measurements, suggesting that R9 might be the dominating deactivation channel within a multi-quantum relaxation scheme in accordance with R8. We therefore included these two conditions in the so-called "O_2 best fit model" and the results are displayed in Fig. 3. The corresponding branching ratios for the individual pathways are summarized in Table 2.

The simulated OH airglow fits well with the three OH airglow observations within the error bars below 85 km. In the altitude region above 85 km, it is seen that the model still overestimates OH(6-2) VER while OH(3-1) VER is indicated to be slightly underestimated. Furthermore, this pattern is not seen in OH(5-3)+OH(4-2) VER and therefore could be attributed to deviations due to the different satellite/instrument configurations between TIMED/SABER and ENVISAT/SCIAMACHY. But since this behaviour only occurs in the upper part of the vertical profiles and is not seen throughout the entire height interval, it is more likely related to O(^{3}P) quenching.

3.3 Deactivation of OH(ν) by O(^{3}P)

Only recently, Sharma et al. (2015) proposed a new pathway of OH(ν)+O(^{3}P) by providing a direct link between higher and lower vibrational levels via:

$$OH(\nu)+O(^3P) \rightarrow OH(0 \leq \nu' \leq \nu-5)+O(^1D) \qquad (R11),$$

with the vibrationally independent reaction constant $k_{11} = 2.3\times10^{-10}$ cm^3 s^{-1}. While the value of $k_{11}(9)$ is based on measurements (Kalogerakis et al., 2011; Thiebaud et al., 2010) and on calculations (Varandas, 2004), the values for $k_{11}(5, 6, 7, 8)$ are only assumed to be identical to $k_{11}(9)$ and should be viewed more critically.

We adapted R11 in the "O_2 best fit O(^{3}P) ν-5 model" in such a way that the product is OH(ν'=ν-5)+O(^{1}D) and the results obtained are displayed as blue lines in Fig. 4. Comparisons for OH(6-2) VER in Fig. 4a show an underestimation of the model at altitudes >85 km. A sensitivity study was carried out which implied that the impact of OH(9,8,7)+O(^{3}P) on OH(6-2) VER is negligible. This seems

reasonable because these three upper states only indirectly influence OH(6-2) via R11. Consequently, our analysis suggests a lower value of $k_{11}(6)$ and best agreement between model output and OH(6-2) VER observations was obtained for an overall rate of approximately 0.8×10^{-10} cm^3 s^{-1}.

In case of OH(5-3)+OH(4-2) VER, presented in Fig. 4b, the new approach leads to a weak underestimation of the observations by the model in the altitude region above 85 km, even if OH(9)+O(^{3}P) of R11 solely populates OH(4). The model results are most sensitive to $k_{11}(5)$, and therefore this rate might be too high. Considering our best fit value obtained for $k_{11}(6)$, it is indicated that $k_{11}(v)$ decreases with decreasing vibrational level. This assumption is supported by the overall rate of OH(7)+O(^{3}P)→OH(v')+O(^{1}D) at mesopause temperature which is suggested to be on the order of $0.9\text{-}1.6\times10^{-10}$ cm^3 s^{-1} (Thiebaud et al., 2010; Varandas, 2004). Thus, an upper limit of $k_{11}(5)<k_{11}(6)$ is recommended and the actual rate coefficient has to balance the direct contribution of OH(9) to OH(4) via R11. Investigating another scenario of $k_{11}(5)$ being zero showed that the branching of OH(9) to OH(4) has to be at least about 0.6 which corresponds to a rate of a $\sim1.4\times10^{-10}$ cm^3 s^{-1}.

It is seen in Fig. 4c that observations and O_2 best fit O(^{3}P) v-5 model output of OH(3-1) VER are in agreement within the corresponding measurement errors but the model values seem to be slightly too low at heights >85 km. In this altitude region, simulated OH(3-1) VER is most influenced by OH(9,8)+O(^{3}P) of R11 because both vibrational levels can directly populate OH(3). However, not much is known about the individual branching ratios of R11 except that OH(9)+O(^{3}P)→OH(3)+O(^{1}D) is an important deactivation channel but not necessarily the dominating one (Kalogerakis et al., 2016). This agrees with our results presented here because the O_2 best fit O(^{3}P) v-5 model only considers a contribution of OH(8) to OH(3) and the underestimation indicated in Fig. 4c could be attributed to the missing channel OH(9)+O(^{3}P)→OH(3)+O(^{1}D). The conclusions drawn from comparisons between three different airglow observations and our model studies with respect to OH(v)+O(^{3}P) quenching are summarized in Table 3.

Finally, all these findings presented in Table 2 and 3 were adapted in the "Best fit model" (Fig. 4, red lines), resulting in an overall agreement between model output and measurements within the corresponding errors. Note that $k_{11}(7)$ used here is the average of the lower and upper limits derived from Thiebaud et al. (2010) and Varandas (2004) which is unlikely to be seriously in error. Furthermore,

it is indicated that the value of $k_{11}(8)$ might be lower than 2.3×10^{-10} cm^3 s^{-1} which can be assumed based on the other rates of $k_{11}(v)$. But we did not find any study reporting an observed $k_{11}(8)$ rate, and consequently we did not change $k_{11}(8)$. Besides, we have to point out that lowering $k_{11}(8)$ does not affect the general conclusions drawn in this section.

The empirically determined solution presented here implies that the contribution of OH(9) to OH(8) via quenching with $O(^3P)$ is close to zero (see Table 1 and this section). In contrast, the model described in Mlynczak et al. (2018) assumes single-quantum relaxation ($OH(9)+O(^3P)\rightarrow OH(8)+O(^3P)$) to get the global annual energy budget into near balance. But applying this approach in our OH model (same total rate of 3×10^{-10} cm^3 s^{-1} and varying the rates for $OH(v\leq8)+O(^3P)$) leads to a considerable overestimation of OH(6-2) VER. Additionally, the shape of simulated OH(5-3)+OH(4-2) VER slightly mismatches the observed OH(5-3)+OH(4-2) VER above 90 km (not shown here). Based on these sensitivity runs, we conclude that at least part of $OH(9)+O(^3P)$ channel has to be deactivated via multi-quantum quenching. This is supported by the results presented by Panka et al. (2017) which adjusted an OH airglow model to fit night-time $CO_2(\nu_3)$ emissions at 4.3 µm. However, this study reported empirically determined rates for $OH(5\leq v\leq8)+O(^3P)$ generally higher than the rates obtained in this work. But these differences might be attributed to their faster values of $OH(v)+O_2$ because they seem to have falsely assumed that the rates of Adler-Golden (1997) do not take mesopause temperature into account. Thus, we think that their rates of $OH(v)+O_2$ are too high, at least by a factor of ~1.5. Since they performed an empirical study, it is not possible to estimate how much this issue affects the rates of $OH(5\leq v\leq8)+O(^3P)$. But we know from our work that higher rates of $OH(v)+O_2$ lead to higher values of OH(6-2) VER, OH(5-2)+OH(4-2) VER, and OH(3-1) VER which can be generally balanced by higher rates of $OH(5\leq v\leq8)+O(^3P)$. Considering our comparisons with these two studies, we think that the rates of $OH(v)+O(^3P)$ should be investigated in more detail in future studies as this rate has a huge impact on derived values of $O(^3P)$ (Panka et al., 2018).

3.4 Derived profiles of $O(^3P)$ and H

Figure 5 displays the vertical profiles of $O(^3P)$ and H obtained by the Best fit model in comparison with the results derived from SABER OH(9-7)+OH(8-6) VER only (Mlynczak et al., 2018). The $O(^3P)$

profiles seen in Fig. 5a agree below 85 km but the Best fit model shows gradually larger values in the altitude region above. These higher values are caused by the different deactivation rates and schemes of OH(v)+O(^{3}P), agreeing with general pattern reported in Panka et al. (2018). We have to point out that other studies (e.g. von Savigny and Lednyts'kyy, 2013) observed a pronounced O(^{3}P) maximum of about 8×10^{11} cm^{-3} at 95 km. The O(^{3}P) derived here indeed shows similar values at 95 km but a maximum is not seen. Nevertheless, the O(^{3}P) in our study obtained above 95 km looks rather unexpected and possible reasons are discussed below.

The night-time H derived in this study shows similar pattern as SABER H, including the maximum at 80 km. But Best fit model H is systematically larger than SABER H by a factor of approximately 1.5. This might be partly caused by too high O_3 night-time values, as suggested by Mlynczak et al. (2018). Similar to the comparisons with O(^{3}P), Best fit model H results also shows unexpected patterns above 95 km.

The quality of the derived profiles is primarily affected by three different uncertainty sources. The first source includes uncertainties due to the rates of chemical and physical processes considered in the Best fit model. We assessed the 1σ uncertainty by assuming uncorrelated input parameters. Adler-Golden (1997) did not state any uncertainties for f_9 and f_8 but these values should be similar to the uncertainty of f_8 derived by Klenerman and Smith (1987). Therefore, we applied an uncertainty of 0.03 for f_9 and f_8.

In case of the Einstein coefficient, we adapted an uncertainty of 10 % as suggested by Mlynczak et al. (2013). All the other 1σ uncertainties of the input parameters were taken from their respective studies. The total 1σ uncertainty was obtained by calculating the root-sum-square of all individual uncertainties. The results of 1σ uncertainty of O(^{3}P) and H derived by the Best fit model are shown as error bars in Fig. 5. The error bars of SABER O(^{3}P) and H were adapted from the corresponding publication.

In case of the Best fit model O(^{3}P) profile, the 1σ uncertainty varies between 20 % and 30 %, depending on altitude. The individual contributions of the input parameters to the total 1σ uncertainty are considerably different. Einstein coefficients and nascent distribution each account for about 5 % throughout the entire height interval. The influence of the collision rates is lower than 6 % and gradually decreases to zero with increasing altitude. In contrast, the chemical reaction rates k_2 and k_3 account for

~85 % to ~90 % of the overall 1σ uncertainty of the derived O(^{3}P) profiles. The total 1σ uncertainty of H also varies between 20 % and 30 % with k_1 being the major uncertainty source (~85 %) below 85 km. In higher altitude regions, the impact due to uncertainty of O(^{3}P) becomes gradually more important and both k_1 and O(^{3}P) each contribute close to one half to the overall uncertainty at altitudes >95 km. We further assumed a worst case scenario (not shown here), meaning that all uncertainties of the input parameters contribute to either higher or lower O(^{3}P) values, obtaining a worst case 1σ uncertainty of approximately 60 % for O(^{3}P) and about 50 % for H. However, it is more likely that the uncertainties are uncorrelated since they originate from independent measurements.

The second aspect influencing the quality of the derived profiles is the assumption of chemical equilibrium of O_3, represented by Eq. (3). This issue was recently investigated by Kulikov et al. (2018), which carried out simulations with a 3-D chemical transport model. They suggested that chemical equilibrium of O_3 is only valid when OH(9-7)+OH(8-6) VER exceeds a certain threshold, depending on *G* and several chemical reactions involving O_x and HO_x species. Applying their suggested limit, we found that in our case chemical equilibrium of O_3 is probably true only above 80 km.

The last problem lies in the fact that the approach used here (see Sect. 2.2) has to be applied to individual OH airglow profiles to derive O(^{3}P) and H correctly. However, the individual scans of OH(6-2) were too noisy to analyze single profiles and we therefore used climatology for all input parameters. By investigating individual OH airglow profiles, we would derive individual O(^{3}P) profiles and eventually average them to the mean O(^{3}P) profile. While in our case, we directly derive the mean O(^{3}P) profile. This makes no difference as long as the relation between OH airglow and O(^{3}P) is a linear one. But Eq. (4b) shows that the relation between O(^{3}P) and OH(9-7)+OH(8-6) VER is only approximately linear because *G* also depends on O(^{3}P), as represented by the terms C_ν and $C_{\nu\nu}$. The linearity between OH(9-7)+OH(8-6) VER and O(^{3}P) of an air parcel with a certain temperature and pressure is solely controlled by O(^{3}P)×G. Note that H too is affected by this non-linearity issue since H depends on *G* (Eq. (4a)). Thus, derived H values are only reliable as long as the derived O(^{3}P), and as a consequence *G*, is not seriously in error.

In order to test the linearity, O(^{3}P)×G was plotted as a function of O(^{3}P) and the corresponding results for Best fit model at five different heights are presented in Fig. 6. It is seen that the relation between

$O(^3P)$ and $O(^3P)\times G$ or OH(9-7)+OH(8-6), respectively, is linear for small values of $O(^3P)$, while a non-linear behaviour becomes more pronounced for larger values of $O(^3P)$. Furthermore, the starting point of the behaviour is shifted to lower $O(^3P)$ values at higher altitudes. In order to estimate this threshold, we performed a visual analysis and determined an upper limit of $O(^3P)$ before non-linearity of $O(^3P)\times G$ takes over. The approximated upper limits are added as dashed lines in Fig. 6. Finally, an $O(^3P)$ value at a certain altitude is assumed to be true if this value is below the corresponding upper limit of $O(^3P)$. Otherwise, it should be viewed more critically. This was done for each altitude and we found that the $O(^3P)$ and H profiles presented in Fig. 5 are plausible in the altitude region <95 km. In combination with the estimation of chemical equilibrium of O_3, we think that the $O(^3P)$ and H derived by the Best fit model provides reasonable results between 80 km and 95 km. Note that these altitude limits do not affect the results with respect to $OH(v)+O_2$ and $OH(v)+O(^3P)$ presented in the Sect. 3.2 and 3.3.

4 Conclusions

We presented a zero dimensional box model which fits the VER of four different OH airglow observations, namely TIMED/SABER OH(9-7)+OH(8-6) and OH(5-3)+OH(4-2) as well as ENVISAT/SCIAMACHY OH(6-2) and OH(3-1). Based on a night-time mean zonal mean climatology of co-location measurements between 2003 and 2011 at 0°-10° N, we found that I) $OH(v)+O_2$ is likely to occur via multi-quantum deactivation while $OH(v\geq7)$ primarily contribute to $OH(v\leq5)$ and might prefer deactivation to $OH(v'=v-5)+O_2$. This relaxation scheme generally agrees with results reported in Russell et al. (2005) but is considerably different to the commonly used scheme suggested by Adler-Golden (1997). We further found II) general support for the new pathway $OH(v)+O(^3P)\rightarrow OH(v')+O(^1D)$ proposed by Sharma et al. (2015) but suggest slower total loss rates of $OH(v=7,6,5)+O(^3P)$. Additionally, hints for a favoured deactivation to $OH(v'=v-5)+O(^1D)$ are obtained. But we have to emphasize that our OH airglow model is based on the transitions OH(9-7)+OH(8-6), OH(6-2), OH(5-3)+OH(4-2), and OH(3-1) only. Thus, our model does not provide any information of $OH(v\leq2)$. Furthermore, it cannot distinguish between OH(5) and OH(4) as well as OH(9) and OH(8), and consequently errors in OH(5) and OH(9) might be compensated by errors in OH(4) and OH(8) or

vice versa. Finally, we have to stress that we performed an empirical model study and the total rates and deactivation channels suggested here heavily depend on the OH transitions considered. Including additional OH transitions might result in other values and deactivation schemes. But these issues will only be solved eventually when future laboratory experiments provide the corresponding $OH(v)+O_2$ and $OH(v)+O(^3P)$ relaxation rates.

Justified by chemical equilibrium of O_3 and a nearly linear relation between $O(^3P)$ and OH(9-7)+OH(8-6) VER, we conclude that the $O(^3P)$ and H profiles derived by the Best fit model are plausible in the altitude range from 80 km to 95 km. The corresponding 1σ uncertainty due to uncertainties of chemical reactions and physical processes varies between 20 % and 30 %, depending on altitude.

Data availability

The data used in this study are open for public. The TIMED/SABER data can be downloaded from http://saber.gats-inc.com/data.php while ENVISAT/SCIAMACHY can be accessed by getting in contact with Christian von Savigny (csavigny@physik.uni-greifswald.de).

Author contribution

MS initialized and supervised the study. CVS retrieved the SCIAMACHY data. TF performed the model runs and wrote the final script with contributions from all co-authors.

Competing interests

The authors declare that they have no conflict of interest.

Acknowledgments

T. Fytterer and M. Sinnhuber gratefully acknowledge funding by the Deutsche Forschungsgemeinschaft (DFG), grant SI 1088/6-1. The authors also acknowledge support by the Open Access Publishing Fund of Karlsruhe Institute of Technology.

References

Adler-Golden, S.: Kinetic parameters for OH nightglow modeling consistent with recent laboratory measurements, J. Geophys. Res., 102, 19,969–19,976, doi:10.1029/97JA01622, 1997.

Anlauf, K. G., MacDonald, R. G., and Polanyi, J. C.: Infrared chemiluminescence from $H+O_3$, at low pressure, Chem. Phys. Lett, 1, 619-622, doi:10.1016/0009-2614(68)80097-1, 1968.

Bovensmann, H., Burrows, J. P., Buchwitz, M., Frerick, J., Noël, S., Rozanov, V. V., Chance, K. V., and Goede, A. P. H.: SCIAMACHY: Mission objectives and measurement modes, J. Atmos. Sci., 56, 127–150, doi:10.1175/1520-0469(1999)056<0127:SMOAMM>2.0.CO;2, 1999.

Bramstedt, K., Noël, S., Bovensmann, H., Gottwald, M., and Burrows, J. P.: Precise pointing knowledge for SCIAMACHY solar occultation measurements, Atmos. Meas. Tech., 5, 2867–2880, doi:10.5194/amt-5-2867-2012, 2012.

Burkholder, J. B., Sander, S. P., Abbatt, J., Barker, J. R., Huie, R. E., Kolb, C. E., Kurylo, M. J., Orkin, V. L., Wilmouth, D. M., and Wine, P. H.: Chemical Kinetics and Photochemical Data for Use in Atmospheric Studies, Evaluation No. 18, JPL Publication 15-10, Jet Propulsion Laboratory, Pasadena, http://jpldataeval.jpl.nasa.gov, 2015.

Burtt, K. D. and Sharma, R. D.: Near-resonant energy transfer from highly vibrationally excited OH to N_2, J. Chem. Phys., 128, 124311-1 to 124311-8, doi:10.1063/1.2884343, 2008.

Caridade, P. J. S. B., Sabin, J., Garridoz, J. D., and Varandas, A. J. C.: Dynamics of OH + O_2 vibrational relaxation processes, Phys. Chem. Chem. Phys., 4, 4959-4969, doi:10.1039/b203101a, 2002.

Caridade, P. J. S. B., Horta, J. Z. J., and Varandas, A. J. C.: Implications of the O + OH reaction in hydroxyl nightglow modeling, Atmos. Chem. Phys, 13, 1-13, doi:10.5194/acp-13-1-2013, 2013.

Chalamala, B. R. and Copeland, R. A.: Collision dynamics of OH($X^2\Pi$, v=9), J. Chem. Phys., 99, 5807-5811, doi:10.1063/1.465932, 1993.

Charters, P. E., Macdonald, R. G., and Polanyi, J. C.: Formation of vibrationally excited OH by the reaction $H+O_3$, Appl. Optics, 10, 1747-1754, doi:10.1364/AO.10.001747, 1971.

Dodd, J. A., Lipson, S. J., and Blumberg, W. A. M.: Formation and vibrational relaxation of OH($X^2\Pi_i$,v) by O_2 and CO_2, J. Chem. Phys., 95, 5752-5762, doi:10.1063/1.461597, 1991.

Dyer, M. J., Knutsen, K., and Copeland, R. A.: Energy transfer in the ground state of OH:

Measurements of OH(v=8,10,11) removal, J. Chem. Phys., 107, 7809-7815, doi:10.1063/1.475094, 1997.

Finlayson-Pitts, B. J. and Kleindienst, T. E.: The reaction of hydrogen atoms with ozone as a source of vibrationally excited $OH(X^2\Pi_i)_{v=9}$ for kinetic studies, J. Chem. Phys., 74, 5643-5658, doi:10.1063/1.440928, 1981.

Good, R. E.: Determination of atomic oxygen density from rocket borne measurements of hydroxyl airglow, Planet. Space Sci., 24, 389–395, doi:10.1016/0032-0633(76)90052-0, 1976.

Gottwald, M., Krieg, E., von Savigny, C., Noël, S., Bovensmann, H., and Bramstedt, K.: Determination of SCIAMACHY Line of Sight Misalignments, Proceedings of the Envisat Atmospheric Science Conference, ESA SP-636, Montreux, Switzerland, 23–27 April, 2007.

Grygalashvyly, M., Sonnemann, G. R., Lübken, F.-J., Hartogh, P., and Berger, U.: Hydroxyl layer: Mean state and trends at midlatitudes, J. Geophys. Res. Atmos., 119, 12,391–12,419, doi:10.1002/2014JD022094, 2014.

Howell, C. D., Michelangeli, D. V., Allen, M., Yung, Y. L., and Thomas, R. J.: SME observations of $O_2(^1\Delta_g)$ nightglow: An assessment of the chemical production mechanisms, Planet. Space Sci., 38, 529-537, doi:10.1016/0032-0633(90)90145-G, 1990.

Kalogerakis, K. S., Smith, G. P., and Copeland, R. A.: Collisional removal of $OH(X^2\Pi, v = 9)$ by O, O_2, O_3, N_2, and CO_2, J. Geophys. Res., 116, D20307, doi:10.1029/2011JD015734, 2011.

Kalogerakis, K. S., Matsiev, D., Sharma, R. D., and Wintersteiner, P. P.: Resolving the mesospheric nighttime 4.3 μm emission puzzle: Laboratory demonstration of new mechanism for OH(υ) relaxation, Geophys. Res. Lett., 43, 8835–8843, doi:10.1002/2016GL069645, 2016.

Kaufmann, M., Lehmann, C., Hoffmann, L., Funke, B., Lopez-Puertas, M., von Savigny, C., and Riese, M.: Chemical heating rates derived from SCIAMACHY vibrationally excited OH limb emission spectra, Adv. Space Res., 41, 1914–1920, doi:10.1016/j.asr.2007.07.045, 2008.

Klenerman, D. and Smith, I. W. M.: Infrared chemiluminescence studies using a SISAM spectrometer, J. Chem. Soc., Farad. T. 2, 83, 229-241, doi:10.1039/F29878300229, 1987.

Knutsen, K., Dyer, M. J., and Copeland, R. A.: Collisional removal of $OH(X^2\Pi)$,v=7) by O_2, N_2, CO_2, and N_2O, J. Chem. Phys., 104, 5798-5802, doi:10.1063/1.471311, 1996.

Kulikov, M. Y., Belikovich, M. V., Grygalashvyly, M., Sonnemann, G. R., Ermakova, T. S., Nechaev, A. A., and Feigin, A. M.: Nighttime ozone chemical equilibrium in the mesopause region. J. Geophys. Res.-Atmos., 123, 1-15, doi:10.1002/2017JD026717, 2018.

Lacoursiere, J., Dyer, M. J., and Copeland, R. A.: Temperature dependence of the collisional energy transfer of OH(ν=10) between 220 and 310 K, J. Chem. Phys., 118, 1661-1667, doi:10.1063/1.1530581, 2003.

López-Puertas, M., García-Comas, M., Funke, B., Picard, R. H., Winick, J. R., Wintersteiner, P. P., Mlynczak, M. G., Mertens, C. J., Russell III, J. M., and Gordley, L. L.: Evidence for an OH(ν) excitation mechanism of CO_2 4.3 µm nighttime emission from SABER/TIMED measurements, J. Geophys. Res., 109, D09307, doi:10.1029/2003JD004383, 2004.

Meinel, A. B.: OH Emission Bands in the Spectrum of the Night Sky. II, Astrophys. J., 112, 120-130, doi:10.1086/145321, 1950.

Mlynczak, M. G. and Solomon, S.: A detailed evaluation of the heating efficiency in the middle atmosphere, J. Geophys. Res., 98, 10,517–10,541, doi:10.1029/93JD00315, 1993.

Mlynczak, M. G., Martin-Torres, F. J., Johnson, D. G., Kratz, D. P., Traub, W. A., and Jucks, K.: Observations of the $O(^3P)$ fine structure line at 63 mm in the upper mesosphere and lower thermosphere, J. Geophys. Res., 109, A12306, doi:10.1029/2004JA010595, 2004.

Mlynczak, M. G., Martin-Torres, F. J., Crowley, G., Kratz, D. P., Funke, B., Lu, G., Lopez-Puertas, M., Russell III, J. M., Kozyra, J., Mertens, C., Sharma, R., Gordley, L., Picard, R., Winick, J., and Paxton, L.: Energy transport in the thermosphere during the solar storms of April 2002, J. Geophys. Res., 110, A12S25, doi:10.1029/2005JA011141, 2005.

Mlynczak, M. G., Hunt, L. A., Mast, J. C., Marshall, B. T., Russell III, J. M., Smith, A. K., Siskind, D. E., Yee, J.-H., Mertens, C. J., Martin-Torres, F. J., Thompson, R. E., Drob, D. P., and Gordley L. L.: Atomic oxygen in the mesosphere and lower thermosphere derived from SABER: Algorithm theoretical basis and measurement uncertainty, J. Geophys. Res.-Atmos., 118, 5724–5735, doi:10.1002/jgrd.50401, 2013.

Mlynczak ,M. G., Hunt, L. A. , Marshall, B. T., Mertens, C. J., Marsh, D. R., Smith, A. K., Russell III, J. M., Siskind, D. E., and Gordley, L. L.: Atomic hydrogen in the mesopause region derived from SABER:

645 Algorithm theoretical basis, measurement uncertainty, and results, J. Geophys. Res.-Atmos., 119, 3516–3526, doi:10.1002/2013JD021263, 2014.

Mlynczak, M. G., Hunt, L. A., Russell III, J. M., and Marshall, B. T.: Updated SABER Night Atomic Oxygen and Implications for SABER Ozone and Atomic Hydrogen, Geophys. Res. Lett., 45, 5735-5741, doi:10.1029/2018GL077377, 2018.

650 Murtagh, D. P., Witt, G., Stegman, J., McDade, J. C., Llewellyn, E. J., Harris, F., and Greer, R. G. H.: An assessment of proposed O(^{1}S) and $O_2(b^1\Sigma_g^+)$ nightglow excitation parameters, Planet. Space Sci., 38, 43-53, doi:10.1016/0032-0633(90)90004-A, 1990.

Nelson Jr., D. D., Schiffman, A., Nesbitt, D. J., Orlando, J. J., and Burkholder, J. B.: H + O_3 Fourier-transform infrared emission and laser absorption sudies of OH($X^2\Pi$) radical: An experimental dipole

655 moment function and state-to-state Einstein A coefficients, J. Chem. Phys., 93, 7003-7019, doi:10.1063/1.459476, 1990.

Ohoyama, H., Kasai, T., Yoshimura, Y., Kimura, H., and Kuwata, K.: Initial distribution of vibration of the OH radicals produced in the H+O_3 → OH($X^2\Pi_{1/2,3/2}$)+O_2 reaction: Chemiluminescence by a crossed beam technique, Chem. Phys. Lett., 118, 263-266, doi:10.1016/0009-2614(85)85312-4, 1985.

660 Panka, P. A., Kutepov, A. A., Kalogerakis, K. S., Janches, D., Russell III, J. M., Rezac, L., Feofilov, A. G., Mlynczak, M. G., and Yigit, E.: Resolving the mesospheric nighttime 4.3 µm emission puzzle: comparing the CO2(ν_3) and OH(ν) emission models, Atmos. Chem. Phys., 17, 9751-9760, doi:10.5194/acp-17-9751-2017, 2017.

Panka, P. A., Kutepov, A. A., Rezac, L., Kalogerakis, K. S., Feolilov, A. G., Marsh, D., Janches, D., and

665 Yigit, E.: Atomic Oxygen Retrieved From the SABER 2.0- and 1.6-µm Radiances Using New First-Principles Nighttime OH(v) Model, Geophys. Res. Lett., 45, 5798-5803, 10.1029/2018GL077677, 2018.

Rensberger, K. J., Jeffries, J. B., and Crosley, D. R.: Vibrational relaxation of OH($X^2\Pi_i$,v=2), J. Chem. Phys., 90, 2174-2181, doi:10.1063/1.456671, 1989.

670 Rothman, L. S., Gordon, I .E., Barbe, A., Benner, D. C., Bernath, P. F., Birk, M., Boudon, V., Brown, L. R., Campargue, A, Champion, J.-P., Chance, K., Coudert, L. H., Danaj, V., Devi, V. M., Fally, S., Flaud, J.-M., Gamache, R. R., Goldmanm, A., Jacquemart, D., Kleiner, I., Lacome, N., Lafferty, W. J., Mandin,

J.-Y., Massie, S. T., Mikhailenko, S. N., Miller, C. E., Moazzen-Ahmadi, N., Naumenko, O. V., Nikitin, A. V., Orphal, J., Perevalov, V. I., Perrin, A., Predoi-Cross, A., Rinsland, C. P., Rotger, M., Simeckova, M., Smith, M. A. H., Sung, K., Tashkun, S. A., Tennyson, J., Toth, R. A., Vandaele, A. C., Vander Auwera, J.: The HITRAN 2008 molecular spectroscopic database, J. Quant. Spectrosc. Ra., 110, 533–572, doi:10.1016/j.jqsrt.2009.02.013, 2009.

Russell, J. P. and Lowe, R. P.: Atomic oxygen profiles (80–94 km) derived from Wind Imaging Interferometer/Upper Atmospheric Research Satellite measurements of the hydroxyl airglow: 1. Validation of technique, J. Geophys. Res., 108, 4662, doi:10.1029/2003JD003454, 2003.

Russell, J. P., Ward, W. E., Lowe, R. P., Roble, R. G., Shepherd, G. G., and Solheim, B.: Atomic oxygen profiles (80 to 115 km) derived from Wind Imaging Interferometer/Upper Atmospheric Research Satellite measurements of the hydroxyl and greenline airglow: Local time–latitude dependence, J. Geophys. Res., 110, D15305, doi:10.1029/2004JD005570, 2005.

Russell III, J. M., Mlynczak, M. G., Gordley, L. L., Tansock, J., and Esplin, R.: An overview of the SABER experiment and preliminary calibration results, in Proceedings of the 44th Annual Meeting, Denver, Colorado, July 18–23, vol. 3756, pp. 277–288, SPIE, Bellingham, WA, 1999.

Sander, R., Baumgaertner, A., Gromov, S., Harder, H., Jöckel, P., Kerkweg, A., Kubistin, D., Regelin, E., Riede, H., Sandu, A., Taraborrelli, D., Tost, H., and Xie, Z.-Q.: The atmospheric chemistry model CAABA/MECCA-3.0, Geosci. Model Dev., 4, 373-380, doi:10.5194/gmd-4-373-2011, 2011.

Shalashilin, D. V., Umanskii, S. Y., and Gershenzon, Y. M.: Dynamics of vibrational energy exchange in collisions of OH and OD radicals with N_2. Application to the kinetics of OH-vibrational deactivation in the upper atmosphere, Chem. Phys., 168, 315-325, doi:10.1016/0301-0104(92)87165-6, 1992.

Shalashilin, D. V., Michtchenko, A. V., Umanskii, S. Y., and Gershenzon, Y. M.: Simulation of Effective Vibrational-Translational Energy Exchange in Collisions of Vibrationally Excited OH with O_2 on the Model Potential Energy Surface. Can the Relaxation of OH(v) Be One-Quantum for Low and Multiquantum for High v?, J. Phys., Chem.-US, 99, 11627-11635, doi:10.1021/j100030a001, 1995.

Sharma, R. D., Wintersteiner, P. P., and Kalogerakis, K. S.: A new mechanism for OH vibrational relaxation leading to enhanced CO_2 emissions in the nocturnal mesosphere, Geophys. Res. Lett., 42, 4639–4647, doi:10.1002/2015GL063724, 2015.

Sharp, W. E. and Kita, D.: In situ measurement of atomic hydrogen in the upper mesosphere, J. Geophys. Res.-Atmos., 92, 4319–4324, doi:10.1029/JD092iD04p04319, 1987.

Smith, A. K., Marsh, D. R., Mlynczak, M. G., and Mast, J. C.: Temporal variation of atomic oxygen in the upper mesosphere from SABER, J. Geophys. Res., 115, D18309, doi:10.1029/2009JD013434, 2010.

Streit, G. E. and Johnston, H. S.: Reactions and quenching of vibrationally excited hydroxyl radicals, J. Chem. Phys., 64, 95-103, doi:10.1063/1.431917, 1976.

Thiebaud, J. E., Copeland, R. A, and Kalogerakis, K. S.: Vibrational relaxation of OH(v=7) with O, O_2 and H, Abstract SA43A-1752, Fall Meeting, AGU, San Francisco, Calif, 2010.

Turnbull, D. N. and Lowe, R. P.: New hydroxyl transition probabilities and their importance in airglow studies, Planet. Space Sci., 37, 723–738, doi:10.1016/0032-0633(89)90042-1, 1989.

Varandas, A. J. C.: Reactive and non-reactive vibrational quenching in O + OH collisions, Chem. Phys. Lett., 396, 182-190, doi:10.1016/j.cplett.2004.08.023, 2004.

Von Savigny, C. and Lednyts'kyy, O.: On the relationship between atomic oxygen and vertical shifts between OH Meinel bands originating from different vibrational levels, Geophys. Res. Lett., 40, 5821-5825, doi:10.1002/2013GL058017, 2013.

Von Savigny, C., McDade, I. C., Eichmann, K.-U., and Burrows, J. P.: On the dependence of the OH* Meinel emission altitude on vibrational level: SCIAMACHY observations and model results, Atmos. Chem. Phys., 12, 8813–8828, doi:10.5194/acp-12-8813-2012 , 2012.

Xu, J., Gao, H., Smith, A. K., and Zhu, Y.: Using TIMED/SABER nightglow observations to investigate hydroxyl emission mechanisms in the mesopause region, J. Geophys. Res., 117, D02301, doi:10.1029/2011JD016342, 2012.

Atmos. Chem. Phys. Discuss., https://doi.org/10.5194/acp-2018-755
Manuscript under review for journal Atmos. Chem. Phys.
Discussion started: 6 August 2018

Atmospheric Chemistry and Physics Discussions

Table 1. Physical processes and chemical reactions included in the Base model

	Process	Rate or scheme	Reference
R1	$H + O_3 \rightarrow OH(\nu) + O_2$	$k_1 = 1.4\times10^{-10}\ e^{(-470/T)}$ $k_1(\nu) = k_1\ f_1(\nu)^a$	Burkholder et al. (2015), Alder-Golden (1997, Table 1)
R2	$O(^3P) + O_3 \rightarrow O_2 + O_2$	$k_2 = 8\times10^{-12}\ e^{(-2060/T)}$	Burkholder et al. (2015)
R3	$O(^3P) + O_2 + M \rightarrow O_3 + M$	$k_3 = 6\times10^{-34}\ (300/T)^{2.4}$	Burkholder et al. (2015)
R4	$OH(\nu) \rightarrow OH(\nu') + h\nu$	variable rates	Xu et al. (2012, Table A1)
R5	$OH(\nu) + N_2 \rightarrow OH(\nu') + N_2$	$\nu'=\nu-1$	Adler-Golden (1997, Table 1), Kalogerakis et al. (2011)
R6	$OH(\nu) + O_2 \rightarrow OH(\nu') + O_2$	$\nu'<\nu$	Adler-Golden (1997, Table 3), see text for more information
R7a	$OH(\nu) + O(^3P) \rightarrow H + O_2$	variable rates	Varandas (2004, Table 3, M I)
R7b	$OH(\nu) + O(^3P) \rightarrow OH(\nu') + O(^3P)$	$\nu'<\nu$	Caridade et al. (2013, Table 1)

[a] $f_1(5, 6, 7, 8, 9) = 0.01, 0.03, 0.15, 0.34, 0.47$

Atmos. Chem. Phys. Discuss., https://doi.org/10.5194/acp-2018-755
Manuscript under review for journal Atmos. Chem. Phys.
Discussion started: 6 August 2018

Atmospheric Chemistry and Physics Discussions

Table 2. Empirically determined branching ratios of $OH(v)+O_2 \rightarrow OH(v')+O_2$ of the O_2 best fit model based on OH(6-2) VER, OH(5-3)+OH(4-2) VER, and OH(3-1) VER observations below 85 km.

v/v'	8	7	6	5	4	3	≤2
9	0	0	0	0	1	0	0
8		0	0	0	0.3	0.7	0
7			0	0	0	0.1	0.9
6				0	0	0	1
5					0	0	1
4						0	1
3							1

Atmos. Chem. Phys. Discuss., https://doi.org/10.5194/acp-2018-755
Manuscript under review for journal Atmos. Chem. Phys.
Discussion started: 6 August 2018

Atmospheric Chemistry and Physics Discussions

Table 3. Empirically determined branching ratios of $OH(v)+O(^3P)\rightarrow OH(v')+O(^1D)$ of the Best fit model based on OH(6-2) VER, OH(5-3)+OH(4-2) VER, and OH(3-1) VER observations above 85 km.

	Process	Recommendation	Best fit rate ($cm^3\ s^{-1}$)
R11a	$OH(9) + O(^3P) \rightarrow OH(4) + O(^1D)$	$k_{11}(9,4) > 0.6\times k_{11}(9)$	$0.8\times2.30\times10^{-10}$
R11b	$OH(9) + O(^3P) \rightarrow OH(3) + O(^1D)$	not negligible	$0.2\times2.30\times10^{-10}$
R11c	$OH(8) + O(^3P) \rightarrow OH(3) + O(^1D)$	not negligible	$0.8\times2.30\times10^{-10}$
R11d	$OH(8) + O(^3P) \rightarrow OH(\leq2) + O(^1D)$	---	$0.2\times2.30\times10^{-10}$
R11e	$OH(7) + O(^3P) \rightarrow OH(\leq2) + O(^1D)$	$k_{11}(7,\leq2) < k_{11}(9)$	1.25×10^{-10}
R11f	$OH(6) + O(^3P) \rightarrow OH(\leq1) + O(^1D)$	$k_{11}(6,\leq1) < k_{11}(9)$	0.80×10^{-10}
R11g	$OH(5) + O(^3P) \rightarrow OH + O(^1D)$	$k_{11}(5) < k_{11}(6)$	0.40×10^{-10}

Atmos. Chem. Phys. Discuss., https://doi.org/10.5194/acp-2018-755
Manuscript under review for journal Atmos. Chem. Phys.
Discussion started: 6 August 2018

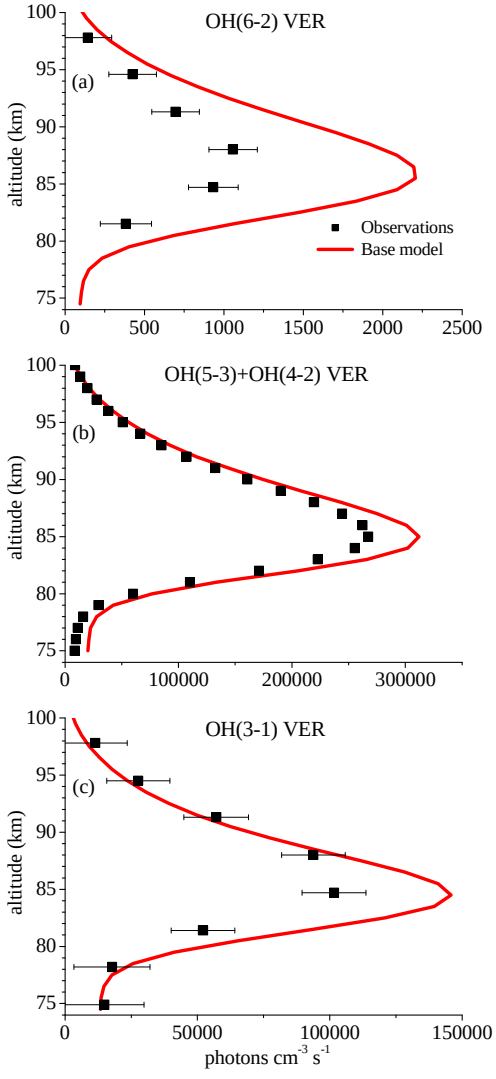

790 **Figure 1 : Comparison of vertical profiles of the volume emission rate (VER) of a) OH(6-2), b) OH(5-3)+OH(4-2), and c) OH(3-1) at 0°-10° N between satellite observations and the Base model output. The observations are climatology of night-time mean zonal means from 2003 to 2011, based on co-location measurements of TIMED/SABER and ENVISAT/SCIAMACHY. Note the different scaling of the x-axis.**

Atmos. Chem. Phys. Discuss., https://doi.org/10.5194/acp-2018-755
Manuscript under review for journal Atmos. Chem. Phys.
Discussion started: 6 August 2018

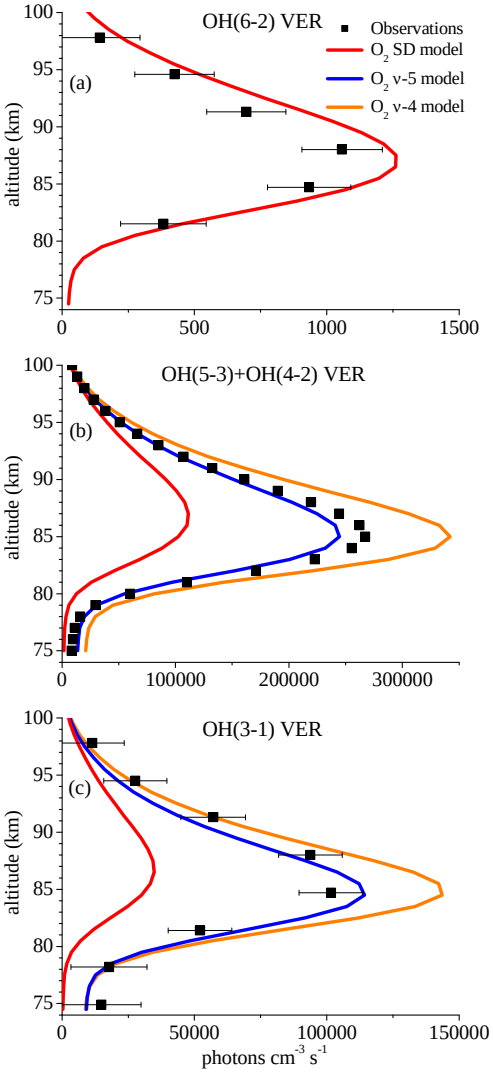

Figure 2 : Same as Fig. 1 but for the O_2 SD model, the O_2 ν-5 model, and the O_2 ν-4 model. Note that the results of these three models are identical in case of OH(6-2) VER.

Atmos. Chem. Phys. Discuss., https://doi.org/10.5194/acp-2018-755
Manuscript under review for journal Atmos. Chem. Phys.
Discussion started: 6 August 2018

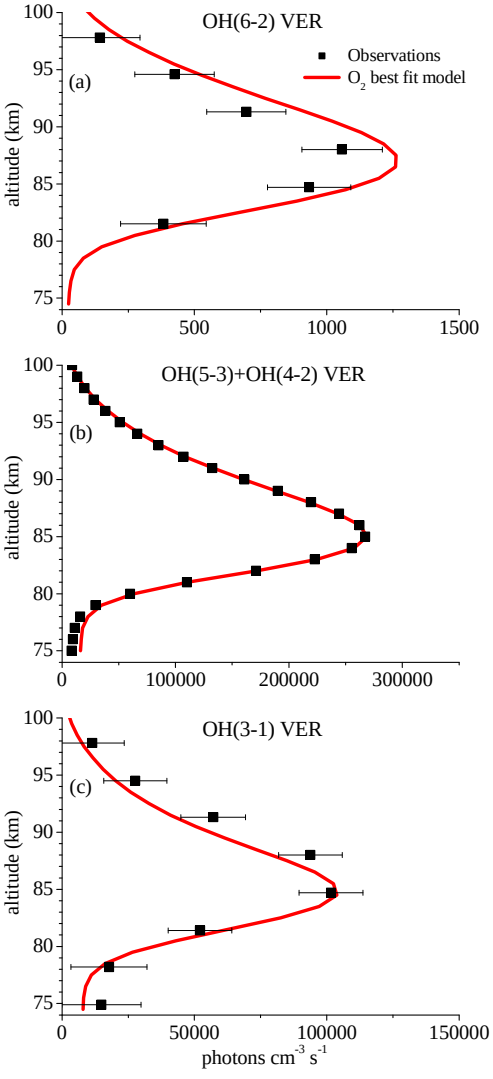

800

Figure 3 : Same as Fig. 1 but for the O_2 best fit model. Note that Fig. 3a is identical to Fig. 2a but was plotted again for convenience.

Atmos. Chem. Phys. Discuss., https://doi.org/10.5194/acp-2018-755
Manuscript under review for journal Atmos. Chem. Phys.
Discussion started: 6 August 2018

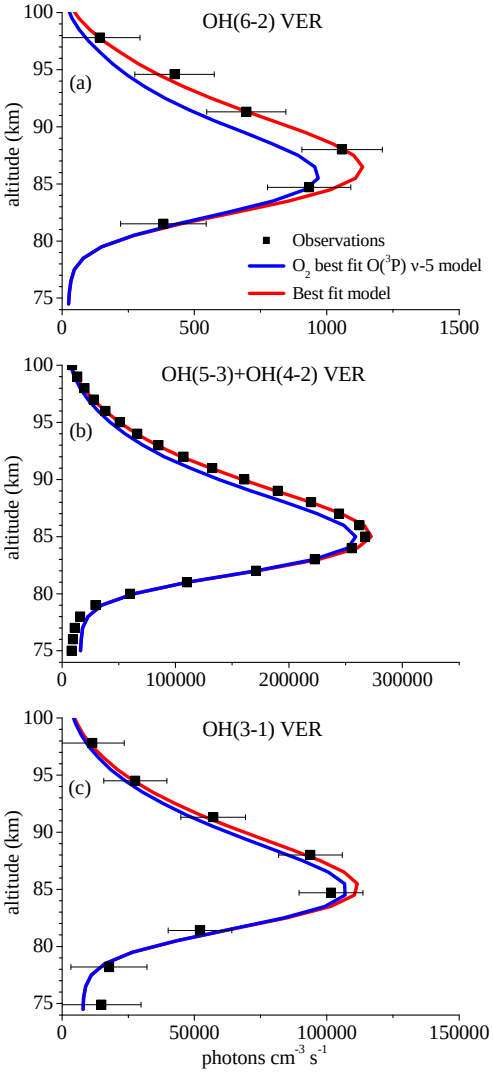

Figure 4 : Same as Fig. 1 but for the O_2 best fit $O(^3P)$ v-5 model and the Best fit model.

Atmos. Chem. Phys. Discuss., https://doi.org/10.5194/acp-2018-755
Manuscript under review for journal Atmos. Chem. Phys.
Discussion started: 6 August 2018

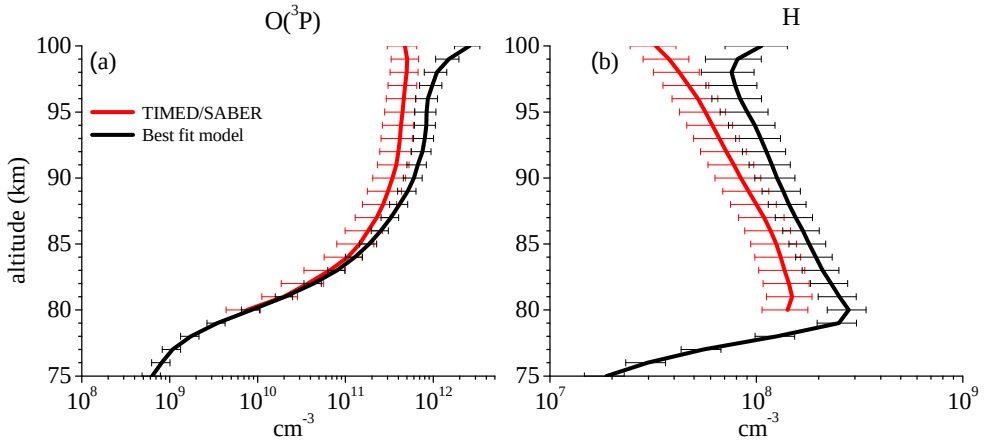

Figure 5 : Vertical profiles of a) $O(^3P)$ and b) H derived from SABER OH(9-7)+OH(8-6) VER observations (Mlynczak et al., 2018) and our Best fit model by fitting SABER OH(9-7)+OH(8-6) VER and OH(5-3)+OH(4-2) VER as well as SCIAMACHY OH(6-2) VER and OH(3-1) VER. Shown are averages of night-time mean zonal means of co-location measurements (see Sect. 2.2) from 2003 to 2011 between 0° and 10° N. Error bars show the 1σ uncertainty due to chemical and physical processes.

Atmos. Chem. Phys. Discuss., https://doi.org/10.5194/acp-2018-755
Manuscript under review for journal Atmos. Chem. Phys.
Discussion started: 6 August 2018

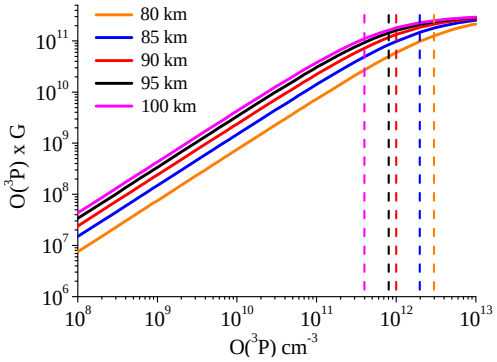

825 **Figure 6 : $O(^3P)\times G$ as a function of $O(^3P)$ at different altitudes. The visually determined upper limits of $O(^3P)$ before non-linearity becomes too pronounced are represented by the dashed lines.**